

Divergent network connectivity changes in behavioural variant frontotemporal dementia and Alzheimer's disease

Juan Zhou,¹ Michael D. Greicius,² Efstathios D. Gennatas,¹ Matthew E. Growdon,¹ Jung Y. Jang,¹ Gil D. Rabinovici,¹ Joel H. Kramer,¹ Michael Weiner,³ Bruce L. Miller¹ and William W. Seeley¹

1 Memory and Aging Center, Department of Neurology, University of California, San Francisco, CA 94117, USA

2 Functional Imaging in Neuropsychiatric Disorders (FIND) Lab, Department of Neurology and Neurological Sciences, Stanford University School of Medicine, Stanford, CA 94305, USA

3 Center for Imaging of Neurodegenerative Diseases, Department of Veterans Affairs Medical Center, San Francisco, CA 94121, USA

Correspondence to: William W. Seeley,
Box 1207, UCSF,
San Francisco,
CA 94143-1207, USA
E-mail: wseeley@memory.ucsf.edu

Resting-state or intrinsic connectivity network functional magnetic resonance imaging provides a new tool for mapping large-scale neural network function and dysfunction. Recently, we showed that behavioural variant frontotemporal dementia and Alzheimer's disease cause atrophy within two major networks, an anterior 'Salience Network' (atrophied in behavioural variant frontotemporal dementia) and a posterior 'Default Mode Network' (atrophied in Alzheimer's disease). These networks exhibit an anti-correlated relationship with each other in the healthy brain. The two diseases also feature divergent symptom-deficit profiles, with behavioural variant frontotemporal dementia undermining social-emotional function and preserving or enhancing visuospatial skills, and Alzheimer's disease showing the inverse pattern. We hypothesized that these disorders would exert opposing connectivity effects within the Salience Network (disrupted in behavioural variant frontotemporal dementia but enhanced in Alzheimer's disease) and the Default Mode Network (disrupted in Alzheimer's disease but enhanced in behavioural variant frontotemporal dementia). With task-free functional magnetic resonance imaging, we tested these ideas in behavioural variant frontotemporal dementia, Alzheimer's disease and healthy age-matched controls ($n = 12$ per group), using independent component analyses to generate group-level network contrasts. As predicted, behavioural variant frontotemporal dementia attenuated Salience Network connectivity, most notably in frontoinsula, cingulate, striatal, thalamic and brainstem nodes, but enhanced connectivity within the Default Mode Network. Alzheimer's disease, in contrast, reduced Default Mode Network connectivity to posterior hippocampus, medial cingulo-parieto-occipital regions and the dorsal raphe nucleus, but intensified Salience Network connectivity. Specific regions of connectivity disruption within each targeted network predicted intrinsic connectivity enhancement within the reciprocal network. In behavioural variant frontotemporal dementia, clinical severity correlated with loss of right frontoinsula Salience Network connectivity and with biparietal Default Mode Network connectivity enhancement. Based on these results, we explored whether a combined index of Salience Network and Default Mode Network connectivity might discriminate between the three groups. Linear discriminant analysis achieved 92% clinical classification accuracy, including 100% separation of behavioural variant frontotemporal dementia and Alzheimer's disease. Patients whose clinical diagnoses were supported by molecular imaging, genetics, or pathology showed 100% separation using this method, including four diagnostically equivocal 'test' patients not used to train the algorithm. Overall, the findings suggest that behavioural variant frontotemporal dementia and Alzheimer's disease lead to divergent network connectivity patterns,

consistent with known reciprocal network interactions and the strength and deficit profiles of the two disorders. Further developed, intrinsic connectivity network signatures may provide simple, inexpensive, and non-invasive biomarkers for dementia differential diagnosis and disease monitoring.

Keywords: functional magnetic resonance imaging; frontotemporal dementia; Alzheimer's disease; functional connectivity; biomarker

Abbreviations: bvFTD = behavioural variant frontotemporal dementia; CDR-SB = Clinical Dementia Rating, sum of boxes score; DMN = Default Mode Network; fMRI = functional magnetic resonance imaging; ICA = independent component analysis; ICN = Intrinsic connectivity network; PIB = Pittsburgh compound B; SFGVAMC = San Francisco Veterans Affairs Medical Center

Introduction

Neurodegenerative diseases target specific neuronal populations within large-scale distributed networks. In early stage disease, region-specific synapse loss, neurite retraction, and gliosis precede neuron loss (Brun *et al.*, 1995) causing neural system dysfunction and symptoms that may anticipate MRI-detectable atrophy. Resting-state or intrinsic connectivity network (ICN) functional magnetic resonance imaging (fMRI) provides a novel tool with the potential to detect disease-related network alterations before brain atrophy has emerged. Furthermore, because cognitive and behavioural functions rely on large-scale network interactions (Mesulam, 1998), ICN fMRI may clarify fundamental aspects of disease pathophysiology. The ICN technique maps temporally synchronous, spatially distributed, spontaneous low frequency (<0.08 Hz) blood-oxygen level-dependent signal fluctuations at rest or, more accurately, in task-free settings (Fox and Raichle, 2007). To date, ICN fMRI has been used to chart normal human and monkey cortical network architecture (Greicius *et al.*, 2003; Beckmann *et al.*, 2005; Fox *et al.*, 2005; Salvador *et al.*, 2005; Damoiseaux *et al.*, 2006; Seeley *et al.*, 2007b; Vincent *et al.*, 2007), predict individual differences in human behaviour and cognition (Hampson *et al.*, 2006; Seeley *et al.*, 2007b; Di Martino *et al.*, 2009b), and confirm that spatial atrophy patterns in five distinct neurodegenerative syndromes mirror normal human ICNs (Seeley *et al.*, 2009). Testing patients directly, ICN analysis has detected predictable connectivity reduction in Alzheimer's disease (Greicius *et al.*, 2004; Rombouts *et al.*, 2005; He *et al.*, 2007; Supekar *et al.*, 2008; Fleisher *et al.*, 2009), prodromal Alzheimer's disease (Rombouts *et al.*, 2005; Sorg *et al.*, 2007), asymptomatic individuals at risk for Alzheimer's disease (Filippini *et al.*, 2009), amyotrophic lateral sclerosis (Mohammadi *et al.*, 2009) and Parkinson's disease (Helmich *et al.*, 2009; Wu *et al.*, 2009); but this technique has not been applied to patients with any frontotemporal dementia syndrome or used to differentiate one disease from another.

Behavioural variant frontotemporal dementia (bvFTD) and Alzheimer's disease, the two most common causes of dementia among patients less than 65 years of age (Ratnavalli *et al.*, 2002), provide a robust conceptual framework for exploring ICN fMRI applications to neurodegenerative disease. Early bvFTD disrupts complex social-emotional functions that rely on anterior peri-allocortical structures, including the anterior cingulate cortex and frontoinsula, as well as the amygdala and striatum (Rosen *et al.*, 2002; Broe

et al., 2003; Boccardi *et al.*, 2005; Seeley *et al.*, 2008a). These regions constitute a large-scale ICN in healthy subjects, which we have referred to as the 'Salience Network' due to its consistent activation in response to emotionally significant internal and external stimuli (Seeley *et al.*, 2007b). Notably, while this anterior network degenerates, posterior cortical functions survive or even thrive, at times associated with emergent visual creativity (Miller *et al.*, 1998; Seeley *et al.*, 2008b). In contrast, Alzheimer's disease often preserves social-emotional functioning, damaging instead a posterior hippocampal-cingulo-temporal-parietal network, often referred to as the 'Default Mode Network' (DMN) (Raichle *et al.*, 2001; Greicius *et al.*, 2003; Buckner *et al.*, 2005; Seeley *et al.*, 2009). DMN-specific functions continue to stir debate, but elements of this system, especially its posterior cortical nodes, participate in episodic memory (Zysset *et al.*, 2002; Buckner *et al.*, 2005) and visuospatial imagery (Cavanna and Trimble, 2006); functions lost early in Alzheimer's disease. Just as bvFTD and Alzheimer's disease show opposing clinical strengths and weaknesses, the Salience Network and DMN show anticorrelated ICN time series (Greicius *et al.*, 2003; Fox *et al.*, 2005; Fransson, 2005; Seeley *et al.*, 2007b), suggesting a reciprocal relationship between these two neural systems. This rich clinical and neuroimaging background led us to hypothesize (as detailed in Seeley *et al.*, 2007a) that bvFTD and Alzheimer's disease would exert opposing influences on the Salience Network and DMN.

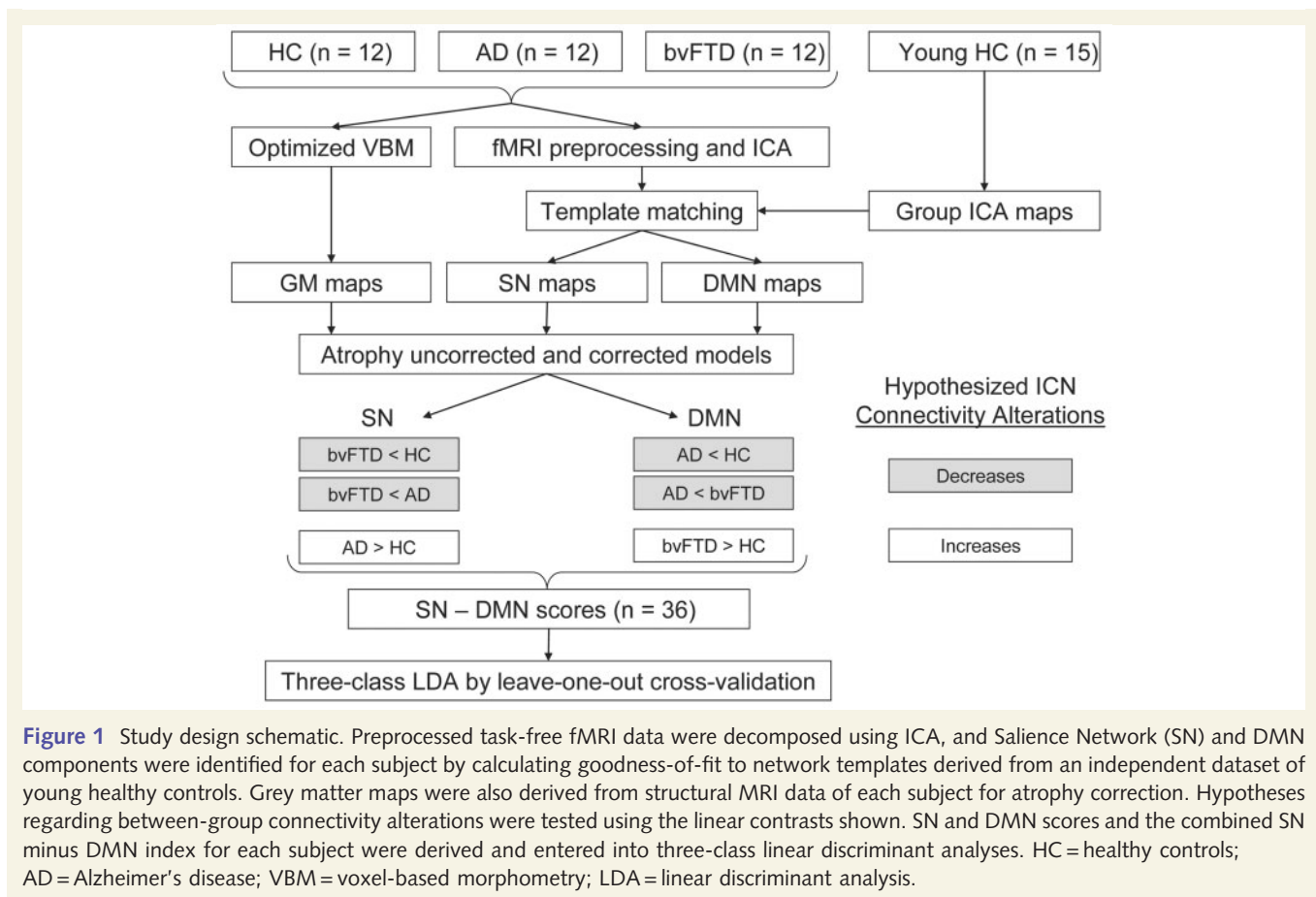
In this study, we used task-free ICN fMRI to demonstrate a divergent effect of bvFTD and Alzheimer's disease on core neural network dynamics. The results provide new insights into the pathophysiology of these disorders and highlight the potential of ICN mapping to provide clinically useful neurodegenerative disease biomarkers.

Materials and methods

Figure 1 provides a schematic summary of the study design and our motivating hypotheses.

Subjects

All subjects (or their surrogates) provided informed consent according to the Declaration of Helsinki and the procedures were approved by the Institutional Review Boards at the University of California, San Francisco (UCSF) and Stanford University. Patients were recruited through the UCSF Memory and Aging Center, where all underwent a comprehensive neurological, neuropsychological and functional



assessment. Final diagnoses were rendered at a multidisciplinary consensus conference, as detailed previously (Rosen *et al.*, 2002). To be considered for inclusion, patients were required to meet published research criteria, which do not include neuroimaging features, for probable Alzheimer's disease (McKhann *et al.*, 1984) and bvFTD (Neary *et al.*, 1998), within 90 days of MRI scanning. In addition, patients were required to have (i) Clinical Dementia Rating (CDR) and Mini-Mental State Examination scores obtained within 180 days of scanning and (ii) absence of significant vascular or other structural lesions on MRI. Finally, because ICN MRI provides an index of brain function that may depend partly on level of consciousness (Kiviniemi *et al.*, 2005), patients were required to tolerate the scanning session without sedation. These requirements slowed bvFTD enrolment due to the behavioural nature of the syndrome. Scanning began at Stanford University but shifted, due to scheduling difficulties, to the San Francisco Veterans Affairs Medical Center (SFVAMC), closer to the primary clinical study site (UCSF). Therefore, we combined patients scanned at the two sites, with five per group scanned at Stanford and seven per group scanned at the SFVAMC to reach our target enrolment of 12 subjects per group. Patients meeting inclusion criteria were scanned as they became available. bvFTD was the last group to reach target fMRI enrolment ($n=12$). At that point, 12 patients with Alzheimer's disease (from 15 available) and 12 healthy controls (from 17 available) were selected to match, as closely as possible, the bvFTD group for age, gender, education and handedness (Table 1). Healthy control subjects were required to have a CDR total score of 0, a Mini-Mental State Examination of 28 or higher, no significant history of neurological disease or structural pathology on MRI, no

neuropsychiatric medications and a consensus diagnosis of cognitively normal within 180 days of scanning. At the time of imaging, three patients with Alzheimer's disease were taking donepezil, and one of these was also taking bupropion. Two patients with bvFTD were taking fluoxetine, including one who was also taking risperidone. Another two patients with bvFTD were taking donepezil, one of whom was also taking duloxetine. No other subjects took neuropsychiatric medications. Medication changes (for example, donepezil initiation in Alzheimer's disease or discontinuation in bvFTD) often take place after imaging at the clinical consensus conference. Because of the diverse medication profiles in each group and the complete confounding of medication with clinical status (patient versus control), we elected not to model medication status in our analyses.

Because clinical syndromic diagnoses can lead to prediction errors regarding underlying histopathology, we collected all available supporting biological data on the patients in this series. These supporting data were not used for subject selection, but were available for a subset of patients selected according to the procedures described above. Three patients with bvFTD had comorbid motor neuron disease, which strongly supports an underlying diagnosis of frontotemporal lobar degeneration with transactivation response element DNA binding protein of 43 kDa (TDP-43) inclusions (Hodges *et al.*, 2004). One of these patients died and showed frontotemporal lobar degeneration with TDP-43, Type 2, at autopsy (Sampathu *et al.*, 2006). One other patient with bvFTD (without motor neuron disease) later died of end-stage disease but did not undergo autopsy. All patients with Alzheimer's disease are living at time of writing. Patients with bvFTD were screened for mutations in disease-causing

Table 1 Subject demographic and neuropsychological features

	Healthy controls	bvFTD	Alzheimer's disease	Overall ANOVA (F, df)	bvFTD/Alzheimer's disease
Age, years	62.0 (89.2)	60.8 (4.6)	63.3 (7.7)	0.4, 35	66.9 (9.9)
M:F, <i>n</i>	5:7	6:6	5:7	$\chi^2 = 0.3, 1$	3:1
Handedness R:L, <i>n</i>	11:1	11:1	11:1	NA	4:0
Education, years	15.8 (3.1)	14.6 (2.2)	15.1 (3.9)	0.41, 35	15.8 (3.1)
Illness duration, years	NA	3.9 (2.0)	4.2 (2.2)	0.18, 22	3.7 (1.3)
CDR, total	0.0 (0.0)	1.0 (0.4) ^h	1.0 (0.4) ^h	24.8, 31	1.1 (0.6)
CDR, sum of boxes	0.0 (0.0)	5.6 (2.2) ^h	5.4 (1.9) ^h	30.6, 31	6.5 (3.1)
MMSE (max = 30)	29.6 (0.7)	25.9 (4.0)	21.2 (5.1) ^{hb}	12.8, 33	25.3 (3.3)
CVLT-SF, four learning trials, total (max = 36)	NC	22.5 (5.8)	17.5 (6.0)	4.0, 22	18.0 (7.3)
CVLT-SF, 10 min recall, score (max = 9)	NC	4.0 (2.8)	1.1 (1.5) ^b	9.2, 22	2.0 (3.4)
Modified Rey-O copy (max = 17)*	15.6 (1.0)	14.4 (1.7)	9.3 (6.4) ^{hb}	6.5, 28	15.3 (1.3)
Modified Rey-O 10 min recall (max = 17)*	11.6 (1.3)	7.4 (3.9) ^h	1.9 (2.2) ^{hb}	23.4, 28	3.8 (5.2)
Digit span backward*	5.4 (1.5)	3.9 (0.9) ^h	3.5 (1.4) ^h	5.4, 29	4.5 (1.9)
Modified trails (correct lines per minute)*	43.5 (20.2)	7.3 (9.9) ^h	19.2 (11.2) ^h	8.2, 29	15.2 (8.9)
Design fluency (correct designs per minute)*	13.5 (2.4)	6.3 (4.2) ^h	3.0 (2.4) ^h	12.5, 21	4.0 (2.9)
Letter fluency ('D' words in 1 min)*	16.6 (1.8)	9.3 (6.6) ^h	8.7 (4.8) ^h	5.7, 29	9.0 (3.8)
Semantic fluency (animals in 1 min)*	21.1 (4.9)	11.8 (5.6) ^h	8.9 (3.7) ^h	14.5, 29	10.3 (6.8)
Abbreviated BNT (max = 15)	14.3 (1.0)	12.3 (2.6)	10.8 (4.4)	2.5, 29	11.0 (3.6)
Calculations (max = 5)*	5.0 (0.0)	4.2 (0.8)	2.8 (1.5) ^{hb}	9.6, 29	3.8 (1.3)
NPI frequency × severity (max = 144)	NC	36.5 (18.1) ^a	20.6 (23.1)	3.2, 20	46.0 (30.6)
NPI, caregiver distress sum (max = 60)	NC	18.7 (10.5) ^a	9.7 (8.7)	4.3, 20	28.7 (20.6)

Values represent mean (SD). Superscript letters indicate whether group mean was significantly worse than healthy controls (h), Alzheimer's disease (a) or bvFTD (b), based on *post hoc* pairwise comparisons ($P < 0.05$). The far right column describes four patients with bvFTD versus Alzheimer's disease who were not entered into the clinical feature ANOVA but were used to test the ICN diagnostic algorithm. Eight measures marked with asterisks were used for three-class classification in linear discriminant analyses.

BNT = Boston Naming Test; CDR = Clinical Dementia Rating; CVLT-SF = California Verbal Learning Test-Short form; MMSE = Mini-Mental State Examination; NA = not applicable; NC = not collected; NPI = Neuropsychiatric Inventory.

genes according to patient wishes, clinical suspicion and availability of these assays at the time of assessment. One patient with bvFTD was found to harbour a mutation in the progranulin gene. No other disease-causing mutations were identified among the nine patients with bvFTD tested for progranulin or the four patients with bvFTD tested for microtubule associated protein tau mutations. Out of 36 subjects, 9 (four with bvFTD, five with Alzheimer's disease) underwent PET imaging with the amyloid- β ligand Pittsburgh compound B (PIB), following previous methods (Rabinovici *et al.*, 2007a). All five patients with Alzheimer's disease were classified as 'PIB-positive', and all four with bvFTD were classified as 'PIB-negative' based on visual rating blinded to clinical diagnosis (Rabinovici *et al.*, 2007a), and these classifications were confirmed using a quantitative threshold for PIB-positivity derived empirically from a contrast of patients with Alzheimer's disease and controls (Aizenstein *et al.*, 2008).

Image acquisition

Structural imaging

Structural MRI scans of five controls, five Alzheimer's disease and five bvFTD subjects (Stanford fMRI subjects) were acquired at the SFVAMC on a 1.5 Tesla Magnetom VISION system (Siemens Inc., Iselin, NJ) using a standard quadrature head coil as previously described (Seeley *et al.*, 2008a). Briefly, a volumetric magnetization prepared rapid gradient echo (MPRAGE) MRI (repetition time/echo time/inversion time = 10/4/300 ms) sequence was used to obtain a T_1 -weighted image of the entire brain (15° flip angle, 154 coronal slices, matrix size 256×256 , $1.0 \times 1.0 \text{ mm}^2$ in-plane resolution of 1.5 mm slab thickness). Structural MRI scans of the remaining seven

controls, seven Alzheimer's disease and seven bvFTD subjects (SFVAMC fMRI subjects) were obtained on a Bruker MedSpec 4.0 Tesla whole body MRI system. A volumetric MPRAGE MRI (repetition time/echo time = 2300/3.37 ms) sequence was used (7° flip angle, 176 sagittal slices, matrix size 256×256 , $1.0 \times 1.0 \text{ mm}^2$ in-plane resolution with a 1.0 mm slab thickness).

Functional imaging

Functional MRI scanning of 15 subjects (Stanford fMRI) was performed at Stanford University. Images were acquired on a 3 Tesla GE Signa Excite scanner (GE Medical Systems, Milwaukee, WI, USA) using a standard GE whole head coil. Twenty-eight axial slices (4 mm thick, 1 mm skip) parallel to the plane connecting the anterior and posterior commissures and covering the whole brain were imaged using a T_2^* -weighted gradient echo spiral pulse sequence (repetition time/echo time = 2000/30 ms; 80° flip angle and 1 interleave). The field of view was $200 \times 200 \text{ mm}^2$, and the matrix size was 64×64 , yielding an in-plane isotropic spatial resolution of 3.125 mm. To reduce blurring and signal loss arising from field inhomogeneities, an automated high-order shimming method based on spiral acquisitions was used before acquiring fMRI scans (Kim *et al.*, 2000). All subjects underwent a 6 min task-free fMRI scan after being instructed only to remain awake with their eyes closed. Functional MRI scanning of the remaining 21 subjects (SFVAMC fMRI) was performed at the SFVAMC on a Bruker MedSpec 4.0 Tesla whole body MRI system. A total of 32 axial slices (3.5 mm thick) parallel to the plane connecting the anterior and posterior commissures and covering the whole brain were imaged using a T_2^* -weighted gradient echo spiral pulse sequence (repetition time/echo time = 2500/30 ms; 90° flip angle and interleaved slicing).

The field of view was $225 \times 225 \text{ mm}^2$, and the matrix size was 64×64 , yielding an isotropic in-plane spatial resolution of 3.52 mm. All subjects underwent a 7.5 min task-free fMRI scan after being instructed only to remain awake with their eyes closed.

Balancing each group for scanner site allowed us to combine subjects across sites within each group while minimizing scanner confounding effects. Furthermore, a previous study showed that site did not play a significant role in explaining the variance in a large task-based fMRI dataset compared to individual variability (Sutton *et al.*, 2008). Nonetheless, especially because our two scanners are of different field strengths, we entered scanner site as a nuisance covariate in all analyses. Similar approaches to merging independent component analysis (ICA)-based, network-oriented analysis of fMRI task data across multiple scanners and field strengths have been reported (Kim *et al.*, 2009).

Image processing and analysis

Structural imaging

To obtain grey matter tissue probability maps for atrophy correction in functional imaging analyses, T_1 -weighted magnetic resonance images underwent an optimized voxel-based morphometry protocol (Good *et al.*, 2001) using Statistical Parametric Mapping-5 (<http://www.fil.ion.ucl.ac.uk/spm/>). First, a study-specific template and tissue priors were created to minimize spatial normalization and segmentation errors. This approach helps to identify group differences in patients with neurodegenerative disease (Senjem *et al.*, 2005). All subjects ($n=36$) were used to create the template, and custom images for each subject were generated by applying affine and deformation parameters obtained from normalizing the grey matter images, segmented in native space, to the custom template. Modulation was performed by multiplying voxel values by the Jacobian determinants derived from the spatial normalization step, and the resulting grey matter maps were smoothed with a 10 mm isotropic Gaussian kernel.

Functional imaging

Preprocessing and ICN derivation

After discarding the first six frames to allow for magnetic field stabilization, functional images were realigned and unwarped, slice-time corrected, normalized and smoothed with a 4 mm full-width at half-maximum Gaussian kernel using SPM5 (<http://www.fil.ion.ucl.ac.uk/spm/>). Normalization was carried out by calculating the warping parameters between the mean T_2^* images and the Montreal Neurological Institute echo planar imaging template and applying them to all images in the sequence. Subsequently, the images were re-sampled at a voxel size of 2 mm^3 .

After preprocessing, we used spatial probabilistic ICA to isolate ICN maps following previous methods (Beckmann and Smith, 2004). ICA decomposes a time course of whole-brain volumes (a 4D image) from a single subject into independent spatiotemporal components and consistently identifies low-frequency ICN patterns from data acquired at various spatial and temporal resolutions (Damoiseaux *et al.*, 2006). Preprocessed images were concatenated into 4D files and entered into FSL 4.0 Melodic ICA software (<http://www.fmrib.ox.ac.uk/fsl/index.html>). We allowed the program to determine the dimensionality of each data set automatically, including the number of components. Across our 36 subjects, ICA extracted an average of 46.3 components (range 28–60; SD 8.5). After removing any components in which high-frequency signal ($>0.1 \text{ Hz}$) constituted 50% or more of the power in the Fourier spectrum, an average of 31.9 components

(range 14–48; SD 8.1) remained. Next, we used an automated template matching procedure to obtain subject-specific best-fit ICN maps for the Salience Network and the DMN (Seeley *et al.*, 2007b, 2009). Goodness-of-fit was calculated by comparing each component from each subject to binarized group ICA maps of the Salience Network and DMN built from 15 healthy young subjects (ages 19–40; mean age, 26.5 years; nine females, all right-handed) from a separate dataset. Details regarding this dataset and corresponding group ICA maps have been published previously (Habas *et al.*, 2009). These ICN templates were thresholded at a z-score ≥ 4.0 to be visually comparable to the consistent ICNs published by Damoiseaux *et al.* (2006). A minor modification of previous goodness-of-fit methods (Seeley *et al.*, 2007b, 2009) was included here for template matching, with goodness-of-fit scores calculated by multiplying (i) the average z-score difference between voxels falling within the template and voxels falling outside the template; and (ii) the difference in the percentage of positive z-score voxels inside and outside the template. This goodness-of-fit algorithm proves less vulnerable to inter-subject variability in shape, size, location and strength of each ICN. Within the selected ICA components, each voxel's z-score represents the degree to which that voxel's time series correlates with the overall component time series. Accordingly, significant group differences at each voxel reflect focal connectivity reduction or enhancement relative to the associated overall ICN.

Group differences in ICN strength

Random effects analyses were performed using each subject's best-fit component images and a 'full factorial' design implemented in SPM5 (Fig. 1). Two-sample *t*-tests were used to generate group difference maps among control, Alzheimer's disease and bvFTD, with scanner site entered as a confounding covariate.

To determine whether observed group differences resulted from underlying grey matter atrophy, we re-analysed each contrast after adding voxel-wise grey matter probability maps as covariates and scanner site as a confounding covariate using the Biological Parametric Mapping toolbox (Casanova *et al.*, 2007). Grey matter probability maps derived from voxel-based morphometry were registered to the same standard image space as the functional images and were re-sampled to equalize voxel sizes and image dimensions across the functional and structural data.

To evaluate further whether and how observed group ICN differences were related to underlying grey matter atrophy, we calculated the correlation between voxel-wise grey matter intensity maps and ICN maps for each network for the 12 bvFTD and 12 Alzheimer's disease subjects, with scanner site entered as a confounding covariate, using the Biological Parametric Mapping toolbox (Casanova *et al.*, 2007).

Correlations between ICN connectivity disruptions and enhancements

Based on the anticorrelated relationship between the Salience Network and DMN (Greicius *et al.*, 2003; Greicius and Menon, 2004; Fox *et al.*, 2005; Seeley *et al.*, 2007a), we further explored whether the identified disease-related connectivity enhancements might correlate with specific regions of reduced ICN strength in whichever network (Salience Network or DMN) did not contain the enhancement. To this end, we first generated 3 mm radius spherical regions of interest centred on the most significant peaks of connectivity enhancement in the group contrast results shown in Fig. 2A and B (second row): left angular gyrus ($-46, -66, 34$) in the DMN bvFTD $>$ controls contrast (centring peak reprinted in Fig. 4A) and right pregenual anterior cingulate cortex ($12, 32, 30$) in the Salience Network Alzheimer's

disease > controls contrast (centring peak reprinted in Fig. 4B). We then extracted the mean ICA component z-scores from within the DMN left angular gyrus region of interest for all bvFTD and control subjects and entered these mean z-scores as covariates of interest in voxel-wise Saliency Network correlation analyses over all 24 subjects, with scanner site entered as a nuisance covariate, seeking regions that exhibited significant negative correlation with the left angular gyrus. Because the Biological Parametric Mapping toolbox is not designed for such correlation analyses, we generated atrophy-corrected results by repeating these analyses after dividing each subject's ICN map by their grey matter map on a voxel-by-voxel basis (Matsuda *et al.*, 2002). For Alzheimer's disease, we conducted a parallel analysis, using the same design skeleton just detailed, seeking instead specific DMN connectivity reductions that correlated with the amplified Saliency Network right pregenual anterior cingulate cortex connectivity observed in Alzheimer's disease > controls.

ICN correlations with bvFTD clinical severity

Clinical severity was assessed using the CDR scale, sum of boxes score (CDR-SB). We chose the CDR-SB because it represents a validated global functional impairment measure, provides a relatively continuous variable and proves sensitive to disease stage in bvFTD (Rosen *et al.*, 2004; Seeley, 2008). Voxel-wise regression analyses were conducted to identify regions whose intrinsic connectivity in each network correlated with CDR-SB. bvFTD and Alzheimer's disease were assessed separately. We predicted that, in bvFTD, regions of worsening Saliency Network connectivity would correlate with increasing CDR-SB, but we also tested for significant correlations (positive or negative) between DMN connectivity and CDR-SB. Similar analyses were conducted for Alzheimer's disease, although we noted that the limited CDR-SB dynamic range in the Alzheimer's disease group would reduce the likelihood of identifying significant correlations. CDR-SB was entered as a covariate of interest, and scanner site was entered as a nuisance covariate. To examine whether identified ICN correlations with CDR-SB were explained by grey matter atrophy alone, we divided each subject's ICN map by their whole brain grey matter map on a voxel-by-voxel basis and repeated the same analyses. To evaluate the strength of the linear relationship between ICN connectivity and clinical severity, we further performed linear regression between CDR-SB and cluster-wise mean z-scores identified in bvFTD.

Linear discriminant analysis of network summary scores

Because our main analyses confirmed that bvFTD and Alzheimer's disease feature divergent effects on the Saliency Network and DMN, we questioned whether a summary score incorporating both ICNs might better differentiate bvFTD from Alzheimer's disease and each patient group from healthy controls. To explore this possibility, we generated a 'Saliency Network minus DMN' index using a four-step procedure. First, to identify the most discriminating regions in this dataset, we performed conjunction analyses on the group-level ICN contrasts to identify regions significant in bvFTD < controls and Alzheimer's disease > controls for the Saliency Network and in Alzheimer's disease < controls and bvFTD > controls for the DMN. Second, we generated 3mm radius spherical regions of interest centred on those peaks identified in the Saliency Network (14 regions) and DMN (eight regions) conjunction analyses. Third, we extracted the mean z-scores for all regions of interest from subjects' Saliency Network and DMN best-fit ICA components. Finally, each subject's Saliency Network minus DMN index was calculated by averaging over all regions of interest in each ICN, subtracting the DMN average from the Saliency Network average and normalizing values across all subjects.

Three-class (controls, bvFTD and Alzheimer's disease) classification using linear discriminant analysis was performed on the Saliency minus DMN index by leave-one-out cross-validation. We used the scores from each of the 36 single subjects as the validation data for classification, and the remaining 35 subjects as the training data to derive linear discriminant models. This procedure was repeated iteratively such that each subject was used once as the validation data, and overall classification performance was calculated based on the 36 single-subject classification results.

Some patients with early age-of-onset dementia present with clinical features falling between the typical bvFTD and Alzheimer's disease profile, leading to diagnostic uncertainty. To begin to assess how well ICN-based classification might perform in this context, we searched our database for patients who (i) met clinical diagnostic research criteria for both bvFTD and Alzheimer's disease; (ii) had undergone an ICN fMRI scan; and (iii) had available pathology, a known disease-causing mutation or a PIB-PET result. Four such patients were identified, all of whom had positive PIB scans and no other supporting data (Table 1). The ICN fMRI acquisition parameters for these subjects were identical in two (one Stanford, one SFVAMC) and featured a slightly longer repetition time in two subjects (SFVAMC) to obtain more complete brain coverage. After performing all preprocessing, ICA and component selection steps identically to the 36 subjects used to train our three-class classification algorithm, we tested this algorithm on the four PIB-positive bvFTD versus Alzheimer's disease subjects.

Statistical thresholding for image analyses

A uniform strategy for statistical image thresholding was employed for all primary analyses, including group-level ICN contrasts, correlations between ICN connectivity disruptions and reciprocal ICN enhancements, and ICN correlations with clinical severity. For these analyses (atrophy uncorrected and corrected), we identified significant clusters using a joint height and extent probability threshold of $P < 0.05$, corrected at whole-brain level (Poline *et al.*, 1997). The statistical maps were masked explicitly to the relevant ICN by binarizing the three-group average ICN at a height threshold of $P < 0.001$ (uncorrected) and including subcortical and brainstem structures (regardless of membership in the three-group average ICN map) to avoid missing focal effects in these finer-grained anatomical regions. The $P < 0.001$ mask threshold was chosen to constrain generously the search volume for group ICN contrasts to regions that compose the relevant ICN without including regions that make up other adjacent ICNs. 'Supplementary Results' regarding the correlation between ICN connectivity and grey matter atrophy employed the same thresholding procedures.

Single-subject ICN scores were derived by using conjunction analyses to identify group-discriminating Saliency Network and DMN regions first. For these conjunction analyses, we applied a liberal height threshold of $P < 0.05$ uncorrected, masked explicitly to the relevant ICN by binarizing to voxels with positive z-scores in the three-group average ICN map. This more liberal threshold served not to test a specific hypothesis but to identify multiple discriminating regions for incorporation into ICN scores.

The Automated Anatomical Labelling toolbox was used to identify the number of grey matter voxels in regions of interest (Tzourio-Mazoyer *et al.*, 2002). For display purposes, all statistical maps are overlaid on a T_1 -weighted Montreal Neurological Institute template using MRICron (<http://www.sph.sc.edu/comd/rorden/mricron/>).

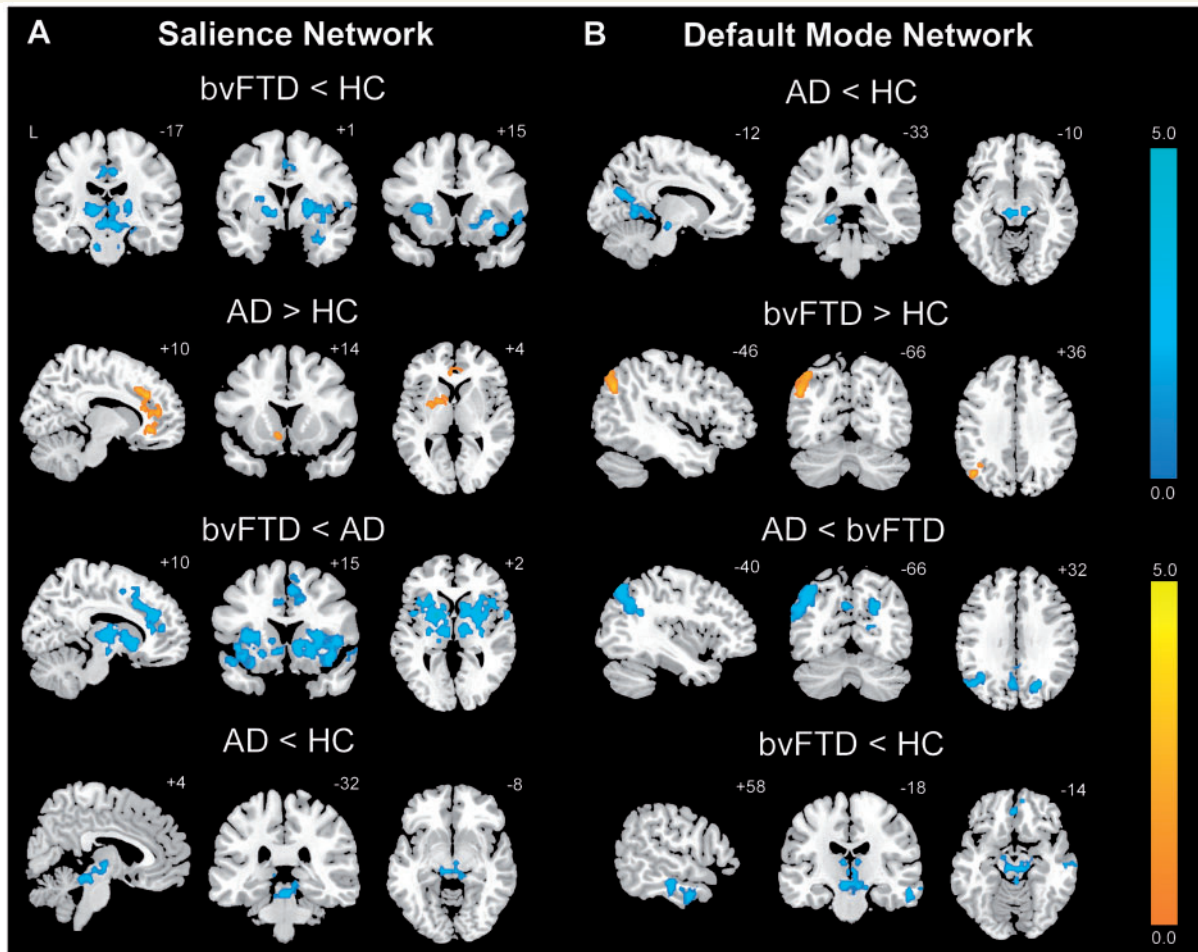


Figure 2 BvFTD and Alzheimer's disease feature divergent Salience Network and DMN dynamics. Group difference maps illustrate clusters of significantly reduced or increased connectivity for each ICN. In the Salience Network (A), patients with bvFTD showed distributed connectivity reductions compared to healthy controls (HC) and patients with Alzheimer's disease (AD), whereas patients with Alzheimer's disease showed increased connectivity in anterior cingulate cortex and ventral striatum compared to healthy controls. In the DMN (B), patients with Alzheimer's disease showed several connectivity impairments compared to healthy controls and patients with bvFTD, whereas patients with bvFTD showed increased left angular gyrus connectivity. Patients with bvFTD and Alzheimer's disease further showed focal brainstem connectivity disruptions within their 'released' network (DMN for bvFTD, Salience Network for Alzheimer's disease). Results are displayed at a joint height and extent probability threshold of $P < 0.05$, corrected at the whole brain level. Colour bars represent t -scores, and statistical maps are superimposed on the Montreal Neurological Institute template brain.

Statistical analyses

Group differences in measures displayed in Table 1 were assessed using the Statistical Package for Social Sciences (SPSS v.17.0), employing analyses of variance (ANOVA) or χ^2 tests as appropriate. All analyses performed in SPSS were considered significant for values of $P \leq 0.05$. To compare the discriminating value of the ICN summary score to standard clinical measures, we also performed a parallel classification analysis on the eight most discriminating neuropsychological measures, those performed on all three groups that featured at least one significant pairwise group difference (Table 1). Three-class linear discriminant analysis using leave-one-out cross-validation was performed on those subjects for whom all discriminating measures were available (7 healthy controls, 10 Alzheimer's disease subjects and 12 bvFTD). We also repeated the ICN-based classification analysis on these same 29 subjects.

Results

BvFTD and Alzheimer's disease feature divergent Salience Network and DMN connectivity changes

BvFTD and Alzheimer's disease present with contrasting deficit and strength profiles and target networks known to adopt an anticorrelated relationship in the healthy brain (Seeley et al., 2007a). Accordingly, we questioned whether these disorders would show opposing patterns of diminished and accentuated intrinsic connectivity within their signature large-scale networks (Seeley et al., 2009). Group-level Salience Network and DMN

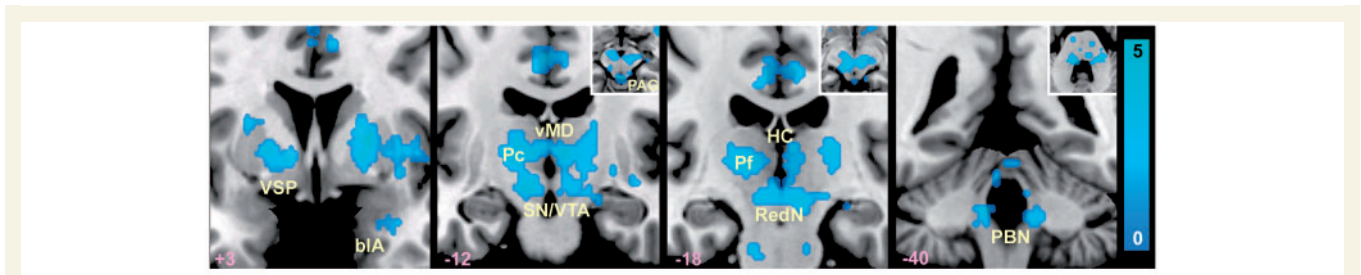


Figure 3 Subcortical and brainstem Saliency Network connectivity reductions in bvFTD. Statistical maps illustrate the Saliency Network contrast of bvFTD < controls. Axial slice insets are provided for selected brainstem regions to clarify cluster locations. bIA = basolateral nucleus of amygdala; Hc = habenular complex; PBN = parabrachial nucleus; Pc = paracentral nucleus of thalamus; Pf = parafascicular nucleus of thalamus; RedN = red nucleus; SN = substantia nigra; vMD = ventral mediodorsal nuclei; VSP = ventral striatopallidum; VTA = ventral tegmental area; PAG = periaqueductal grey matter. Presentation details otherwise as in Fig. 2.

contrasts (Fig. 2 and Supplementary Tables 1 and 2) revealed connectivity reduction and enhancement patterns consistent with our hypotheses. Compared to healthy controls, patients with bvFTD featured decreased cortical Saliency Network connectivity in right frontoinsula, left dorsal anterior insula, right superior temporal pole and bilateral mid-cingulate cortices (Fig. 2A and Supplementary Table 1). Strikingly, patients with bvFTD further showed extensive Saliency Network connectivity disruptions in subcortical, limbic and brainstem structures (detailed in Fig. 3), including the nucleus accumbens and ventral striatopallidum, thalamus (in the vicinity of the parafascicular, paracentral and ventral mediodorsal nuclei bilaterally), habenular complex, hypothalamus, basolateral amygdala/anterior hippocampus, substantia nigra/ventral tegmental area, parabrachial nucleus and pontine and medullary regions. Within the DMN, however, patients with bvFTD showed increased connectivity in left angular gyrus (Fig. 2B and Supplementary Table 2). Conversely, patients with Alzheimer's disease showed reduced DMN connectivity compared to controls in left retrosplenial cortex/lingual gyrus, left posterior hippocampus, left cuneus and midbrain tegmentum, in the vicinity of the dorsal raphe nucleus (Fig. 2B) but increased Saliency Network connectivity versus controls in bilateral anterior cingulate cortex and left ventral striatum (Fig. 2A). When compared to each other, patients with bvFTD and Alzheimer's disease showed similar but more extensive differences than observed in the contrasts between each patient group and controls. That is, bvFTD showed dramatic Saliency Network connectivity reduction compared to Alzheimer's disease, whereas in Alzheimer's disease the DMN was markedly disconnected compared to bvFTD, especially in medial and lateral parietal regions. Critically, in no region did patients with bvFTD show increased Saliency Network connectivity compared to those with Alzheimer's disease or controls (Supplementary Table 1). Likewise, in patients with Alzheimer's disease, no regions showed increased DMN connectivity compared to controls and only the dorsal caudate showed increased DMN connectivity compared to patients with bvFTD (Supplementary Table 2). Together, these findings suggest the following symmetrical patterns: Saliency Network = bvFTD < controls < Alzheimer's disease and DMN = Alzheimer's disease < controls < bvFTD, supporting a 'reciprocal networks' model to explain the divergent

clinical and network features seen in these two disorders (Seeley *et al.*, 2007a).

Despite the observed ICN enhancements (bvFTD in DMN and Alzheimer's disease in Saliency Network), we detected overlapping focal midbrain, epithalamic and thalamic connectivity reductions in each patient group compared to healthy controls within the network showing cortical connectivity enhancement for that group (Fig. 2A and B, bottom row). More specifically, in the Saliency Network Alzheimer's disease showed reductions in posterior hypothalamus and dorsal midbrain/periaqueductal grey matter. Likewise, in the DMN bvFTD showed connectivity disruption in the midbrain tegmentum, habenular complex, tectum/periaqueductal grey matter and the dorsomedial thalamus and hypothalamus.

After atrophy correction, most regions remained significant in all Saliency Network contrasts (Supplementary Table 1 and Supplementary Fig. 1). In the DMN contrasts, all detected regions remained significant after atrophy correction (Supplementary Table 2 and Supplementary Fig. 1). To explore the relationship between grey matter volume and ICN connectivity further, we built correlation maps of these two measures across all 24 patients and compared these maps to the regions whose connectivity reductions were affected by atrophy correction (Supplementary Materials and Supplementary Fig. 1).

ICN enhancements relate to specific connectivity disruptions within the reciprocal network

The reciprocal networks model predicts that ICN enhancements in one network may relate to specific disruptions in the other (reciprocal) network. To test this idea, we sought Saliency Network regions, in bvFTD and controls, whose connectivity strength correlated inversely with connectivity in the left angular gyrus, a DMN region showing enhanced connectivity in bvFTD (Fig. 2B). As highlighted in Fig. 4A, DMN left angular gyrus connectivity was inversely correlated with Saliency Network connectivity in the right frontoinsula/putamen (peak = 56, 0, 8; $t = 3.36$; cluster size = 337), anterior mid-cingulate cortex (peak = 6, -12, 54; $t = 3.78$; cluster size = 650) and bilateral dorsal pontine regions

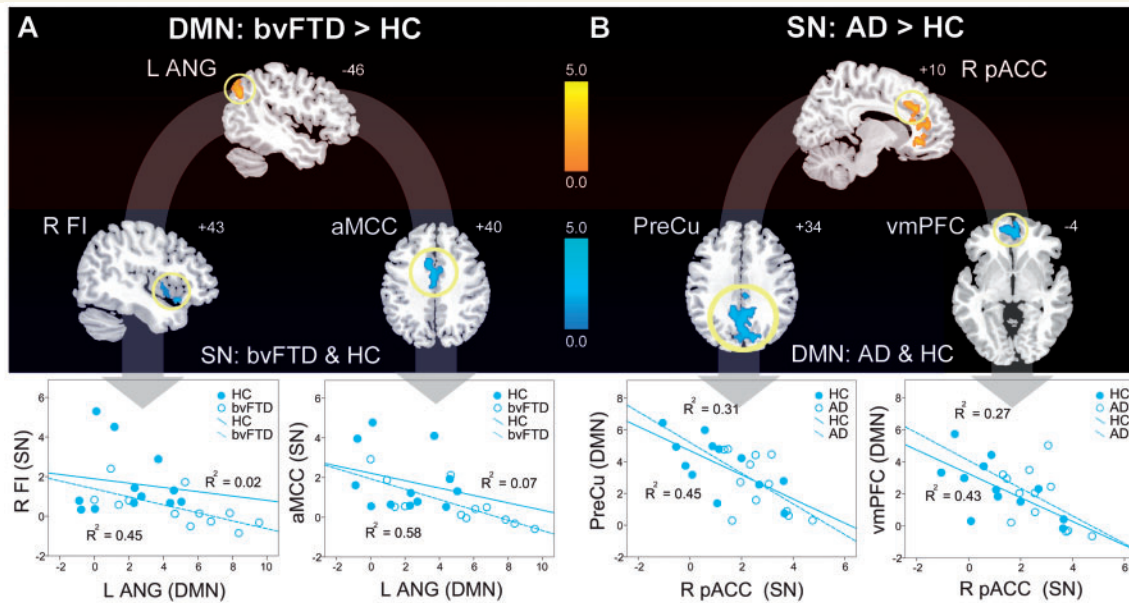


Figure 4 ICN enhancements relate to specific connectivity disruptions within the reciprocal networks. **(A)** Left angular gyrus (L ANG) DMN connectivity was intensified in patients with bvFTD versus healthy controls and the 3 mm radius spherical region of interest centred on its peak showed a significant inverse correlation with SN connectivity in right frontoinsula (R FI), anterior mid-cingulate cortex (aMCC) and the dorsal pons (not shown) across patients with bvFTD and healthy controls (HC). Group-wise scatterplots illustrate the relative contribution of each group to these relationships for each anticorrelated region. **(B)** Right pregenual anterior cingulate cortex (R pACC) SN connectivity, enhanced in patients with Alzheimer's disease (AD), showed a significant inverse relationship with DMN connectivity in precuneus (PreCu), ventromedial prefrontal cortex (vmPFC) and bilateral middle temporal gyrus (not shown) across patients with Alzheimer's disease and healthy controls. Results are atrophy-corrected and thresholded at a joint height and extent probability of $P < 0.05$, corrected at the whole brain level. Colour bars represent t -scores, and statistical maps are superimposed on the Montreal Neurological Institute template brain.

in the vicinity of the parabrachial nuclei (peak = $-8, -28, -42$; $t = 3.81$; cluster size = 364). Similarly, Fig. 4B reveals that right pregenual anterior cingulate cortex, the Saliency Network region enhanced in Alzheimer's disease (Fig. 2A), correlated inversely, in both Alzheimer's disease and controls, with regions throughout the DMN, including ventral medial prefrontal cortex (peak = $4, 64, 4$; $t = 4.57$; cluster size = 1418), precuneus/posterior cingulate cortex/cuneus (peak = $-16, -74, 20$; $t = 4.23$; cluster size = 2257), left middle temporal gyrus (peak = $-60, -18, -20$; $t = 4.04$; cluster size = 342) and right middle temporal gyrus (peak = $60, -22, -30$; $t = 3.53$; cluster size = 284). Scatterplots in Fig. 4 illustrate the relative contributions of the patient and control groups to each reciprocal network relationship. Overall, these findings suggest that specific connectivity disruptions within each network may enhance connectivity within the reciprocal network.

Saliency Network disruption and DMN enhancement correlate with the clinical severity of bvFTD

Having demonstrated Saliency Network connectivity disruptions and DMN connectivity enhancements in bvFTD, we sought those regions in each network that significantly correlated with bvFTD clinical severity after atrophy correction. As illustrated in

Fig. 5A, CDR-SB correlated with selective connectivity reduction in the right frontoinsula (peak = $46, 20, -2$; $t = 6.50$; cluster size = 712). In contrast, clinical severity showed a positive correlation with DMN connectivity, including left angular gyrus (peak = $-58, -68, 22$; $t = 3.96$; cluster size = 313), right angular gyrus (peak = $50, -48, 12$; $t = 4.82$; cluster size = 287), ventral medial prefrontal cortex (peak = $8, 58, 12$; $t = 9.49$; cluster size = 720) and right intraparietal sulcus (peak = $30, -76, 30$; $t = 5.41$; cluster size = 173) (Fig. 5B). R-square coefficients with respect to CDR-SB were computed from raw mean cluster-wise ICN z-scores, defined in atrophy-corrected models (Fig. 5). In the reverse direction, no regions negatively correlated with bvFTD clinical severity in the DMN, and only one region positively correlated with clinical severity in the Saliency Network, but the majority of this cluster was rooted in deep subfrontal white matter. No correlations between CDR-SB and Saliency Network or DMN connectivity were detected in Alzheimer's disease, most likely due to the limited CDR-SB dynamic range in this group.

Three-class classification of controls, bvFTD and Alzheimer's disease based on intrinsic connectivity

To evaluate the potential of ICN mapping to differentiate between controls, patients with bvFTD and patients with Alzheimer's

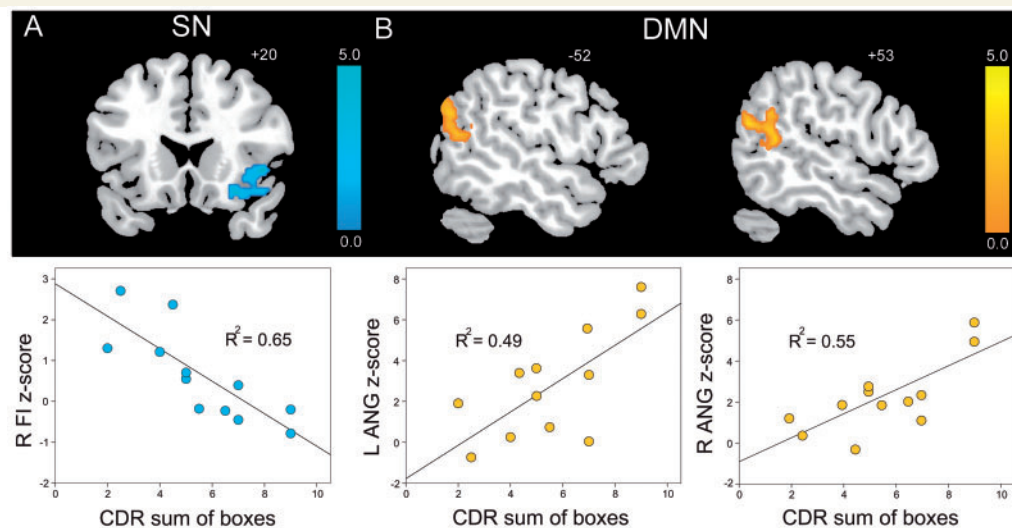


Figure 5 Saliency Network disruption and DMN enhancement correlate with bvFTD clinical severity. In bvFTD, CDR, sum of boxes scores (CDR-SB) showed a significant (A) negative correlation with Saliency Network connectivity in right frontoinsula (FI) and (B) positive correlation with DMN connectivity in bilateral angular gyrus (ANG), as well as ventromedial prefrontal cortex (vmPFC) and right intraparietal sulcus (R IPS, not shown). Results are atrophy corrected and thresholded at a joint height and extent probability of $P < 0.05$, corrected at the whole brain level. Colour bars represent t -scores, and statistical maps are superimposed on the Montreal Neurological Institute template brain.

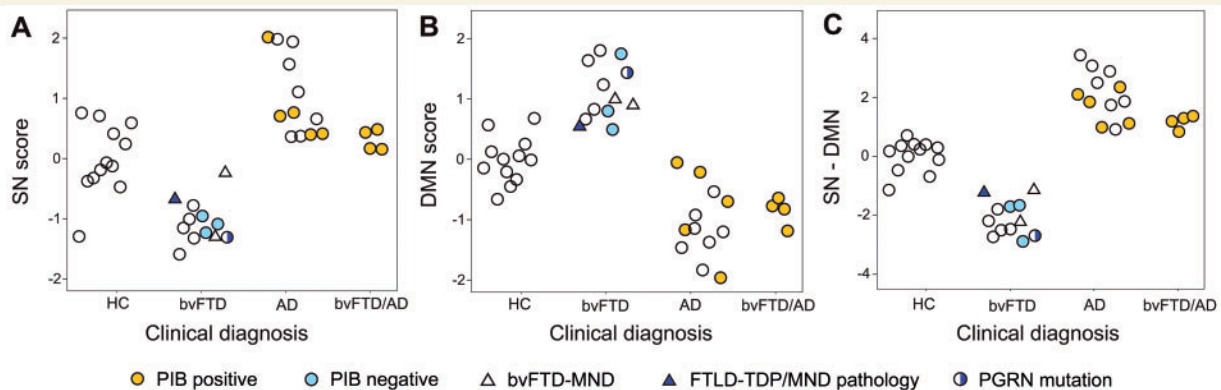


Figure 6 Group discrimination using Saliency Network and DMN metrics. (A) Scatterplot of Saliency Network (SN) scores of healthy controls (HC), patients with bvFTD and Alzheimer's disease (AD) with respect to clinical diagnosis. Each subject's Saliency Network score represents the average z-score across fourteen regions of interest derived from a Saliency Network (bvFTD < healthy control) + (Alzheimer's disease > healthy control) conjunction analysis (Supplementary Table 3). (B) DMN scores were computed in a parallel fashion, using eight regions of interest derived from a DMN (Alzheimer's disease < healthy control) + (bvFTD > healthy control) conjunction analysis (Supplementary Table 3). (C) The combined Saliency Network minus DMN index provided superior group discrimination compared to analysis of either network alone. Dot columns were converted to clouds by random number assignment within each group to improve scatter visualization. Key for colours and shapes is provided at the bottom.

disease, we identified the most group-discriminating regions in our dataset for each ICN (listed for each network in Supplementary Table 2) and derived each subject's corresponding Saliency Network score, DMN score, and a combined index of Saliency Network minus DMN connectivity. Grouped scatter plots (Fig. 6) revealed that combining Saliency Network and DMN scores achieved the best separation among the three groups and 100% separation between bvFTD and Alzheimer's disease. Linear

discriminant analyses of three-class classification based on the combined Saliency Network minus DMN index confirmed the utility of this technique. Table 2 summarizes the classification results of the leave-one-out cross-validation. ICN analysis achieved 92% total three-class classification accuracy, as well as excellent sensitivity and specificity for bvFTD and Alzheimer's disease.

Neuropathological assessment remains the ideal gold standard for dementia diagnostic biomarker development. Novel biomarkers

Table 2 Healthy controls, bvFTD and Alzheimer's disease three-class classification accuracy of Salience Network minus DMN scores by leave-one-out cross-validation

Group	Predicted group			Total
	Healthy controls	bvFTD	Alzheimer's disease	
Healthy controls	11	1	0	12
bvFTD	0	12	0	12
Alzheimer's disease	2	0	10	12
Sensitivity (%)	91.7	100	83.3	91.7
Specificity (%)	91.7	95.8	100	95.8

like ICN mapping, however, must often be assessed without neuropathological confirmation due to the typical interval (5–8 years) between diagnosis and death. Therefore, to add weight to the clinical diagnoses that served as entry criteria for this study, we gathered all supportive biological data available for this series and included these data in Fig. 6. Although unknown to clinicians at the time of diagnosis, these data supported the clinical diagnoses without exception. Patients with biological support were spread throughout their respective group distributions for each ICN measure.

To compare the discriminating value of the Salience Network minus DMN score to standard clinical measures, we further performed a three-class classification analysis on the eight most discriminating neuropsychological measures for a subset of our subjects for whom these measures were uniformly available (7 normal controls, 10 Alzheimer's disease and 12 bvFTD). This classification achieved 66% accuracy. In contrast, Salience Network minus DMN scores achieved 90% accuracy when used to classify the same 29 subjects.

Finally, we explored whether the ICN algorithm might help to resolve diagnostic controversies between bvFTD and Alzheimer's disease. Four patients with multi-domain cognitive impairment and severe behavioural symptoms (Table 1) met clinical research criteria for both disorders but showed extensive amyloid binding on PIB-PET imaging, most consistent with a pathological diagnosis of Alzheimer's disease. These patients, though not used to train the ICN algorithm, fell within the low end of the Alzheimer's disease Salience Network minus DMN distribution, well above the bvFTD range. Three of four subjects were categorized as Alzheimer's disease in three-class classification (one misclassified as a healthy control), but, more importantly, all four were categorized as Alzheimer's disease in two-class (bvFTD versus Alzheimer's disease) classification, corresponding well with the PIB-PET results. Just as patients with Alzheimer's disease may have significant behavioural symptoms, a subset with bvFTD, especially those with progranulin mutations (Rohrer *et al.*, 2008) shows prominent parietal deficits, which could undermine ICN-based classification. In this study, the one patient with a progranulin mutation showed severe parietal involvement (Supplementary Fig. 2) but still fell safely within the bvFTD ICN spectrum (Fig. 6).

Discussion

We used task-free ICN fMRI to show that bvFTD and Alzheimer's disease result in divergent, indeed opposing patterns of large-scale network connectivity. Although previous studies have demonstrated ICN disruptions in Alzheimer's disease (Greicius *et al.*, 2004; Rombouts *et al.*, 2005; He *et al.*, 2007; Sorg *et al.*, 2007; Fleisher *et al.*, 2009) and other neurodegenerative disorders (Mohammadi *et al.*, 2009; Wu *et al.*, 2009), this study is the first to apply ICN analysis to bvFTD, or to compare two neurodegenerative diseases with each other. Consistent with our hypotheses, bvFTD undermined the Salience Network, a distributed anterior ICN dedicated to social-emotional and viscerautonomic processing (Seeley *et al.*, 2007b; Taylor *et al.*, 2009), but intensified connectivity within a posterior DMN involved in episodic memory and visuospatial functions (Greicius *et al.*, 2003; Buckner *et al.*, 2005). Alzheimer's disease, conversely, showed DMN reductions but Salience Network enhancements. These reciprocal findings parallel the clinical deficit-strength profiles in bvFTD and Alzheimer's disease (Seeley *et al.*, 2007a) and the Salience Network-DMN anti-correlation relationship in the healthy brain (Greicius *et al.*, 2003; Fox *et al.*, 2005; Fransson, 2005; Seeley *et al.*, 2007a). Furthermore, specific 'disconnections' within each disease-targeted network predicted ICN enhancements within the reciprocal network. Congruently, advancing bvFTD severity correlated with reduced Salience Network connectivity in the right frontoinsula but with enhanced biparietal DMN connectivity. Focal atrophy, especially when severe, accentuated connectivity reductions in bvFTD, but voxel-wise atrophy correction methods also confirmed that most ICN group differences could not be explained by atrophy alone. To explore ICN mapping as a diagnostic biomarker, we identified group-discriminating ICN changes in this dataset and used them to achieve 92% overall three-group diagnostic classification accuracy and 100% separation between bvFTD and Alzheimer's disease, even among patients with tenuous clinical diagnoses. The findings suggest that ICN assays, further developed, could become powerful tools in translational neuroscience research.

Reciprocal networks: bvFTD and Alzheimer's disease cause opposing ICN alterations

Salience Network

Early bvFTD disrupts complex social-emotional functions, including self-conscious emotion (Sturm *et al.*, 2006, 2008), theory of mind (Eslinger *et al.*, 2005; Lough *et al.*, 2006), empathy (Rankin *et al.*, 2005) and emotional morality (Mendez and Shapira, 2009). These deficits arise in parallel with early (Broe *et al.*, 2003; Seeley *et al.*, 2008a), consistent (Schroeter *et al.*, 2008) and progressive (Brambati *et al.*, 2007) atrophy within Salience Network affiliated regions. We detailed the Salience Network in healthy young (Seeley *et al.*, 2007b) and older (Seeley *et al.*, 2009) controls, in part to provide an anatomical roadmap for bvFTD investigation. In this study, we discovered that bvFTD interrupts Salience Network

connectivity, most notably in the frontal and anterior insula, mid-cingulate and numerous subcortical, limbic and brainstem nodes with known anatomical connectivity to Salience Network cortical regions in primates (Mesulam and Mufson, 1982; Ongur and Price, 2000; Saper, 2002; Heimer and Van Hoesen, 2006). The right frontoinsula, in particular, may serve as a critical Salience Network hub (Sridharan *et al.*, 2008) that anchors subjective awareness through multichannel integration of contextual (temporal pole), hedonic (nucleus accumbens, ventral striatopallidum), homeostatic (amygdala, hypothalamus) and interoceptive (parabrachial nucleus) processing streams (Damasio, 2003; Craig, 2009a, b). In early bvFTD, distributed Salience Network connectivity reductions may disintegrate these complex viscerosomatic and social-emotional signals, resulting in degraded self-representations and impaired social behaviour.

Although patient strengths are rarely cited as important dementia diagnostic clues (Miller *et al.*, 2000), preserved social graces and interpersonal warmth often lead experienced clinicians to suspect Alzheimer's disease in a patient with mild memory or visuospatial complaints. Remarkably, we found that Alzheimer's disease produces heightened Salience Network connectivity in anterior cingulate cortex and ventral striatum compared with healthy elderly controls. But what evidence supports Salience Network functional gains in Alzheimer's disease? Often, early-stage patients exhibit heightened emotional sensitivity to others and to their own cognitive deficits, avidly seeking eye contact with their caregivers, and even patients with advanced disease remain attuned to non-verbal emotional communication (Belgrave, 2009). Behavioural symptoms, when present, often involve early emotional sensitizations such as irritability and anxiety (Mega *et al.*, 1996; Benoit *et al.*, 1999), the latter previously linked to heightened Salience Network anterior cingulate cortex connectivity in healthy young subjects (Seeley *et al.*, 2007b). In experimental settings, patients with Alzheimer's disease show preserved sensitivity to salient social-emotional cues (Rankin *et al.*, 2006; Mendez and Shapira, 2009) and exaggerated anterior cingulate cortex responses to nociceptive stimuli (Cole *et al.*, 2006). A previous graph theoretical analysis of a different ICN fMRI dataset showed frontal intrinsic connectivity enhancements in Alzheimer's disease (Supekar *et al.*, 2008), including heightened frontostriatal connectivity. The anterior cingulate cortex and frontoinsula, moreover, stand out as the sole regions to show increased grey matter volume in pathologically diagnosed Alzheimer's disease compared to frontotemporal lobar degeneration (Rabinovici *et al.*, 2007b). Like patients with Alzheimer's disease, children with Williams Syndrome, a neurodevelopmental disorder resulting from a chromosome 7q11.23 microdeletion, show heightened sociality, trait anxiety and severe parietal visuoconstructive deficits (Meyer-Lindenberg *et al.*, 2006), further supporting a reciprocal relationship between anterior social and posterior spatial networks. In the present study, heightened Salience Network connectivity in Alzheimer's disease was associated with reduced connectivity throughout the DMN, suggesting that progressive DMN impairment may shift Salience Network responses from sensitive to oversensitive, resulting in worsening anxiety and agitation with advancing disease. Future studies could directly assess whether Salience Network connectivity enhancements explain the striking

social-emotional sensitivity, sometimes overflowing towards anxiety, seen in patients with Alzheimer's disease.

Default Mode Network

Early Alzheimer's disease-related memory lapses, navigational errors, and disrupted visuoconstructive processing may relate to specific focal disruptions in posterior temporal and parietal circuits identified in this study. We further report Alzheimer's disease-related DMN connectivity reduction in or near the dorsal raphe nucleus, which projects extensively to the medial temporal lobe and represents an early (Rub *et al.*, 2000), if not the earliest (Grinberg *et al.*, 2009), site of Alzheimer's disease-related tau neurofibrillary pathology. These clinicoanatomical deficits contrast sharply with bvFTD, which typically spares (Mendez *et al.*, 1996) or, less often, intensifies (Miller *et al.*, 1996, 2000; Seeley *et al.*, 2007a) visuospatial interest and ability. In one patient with progressive non-fluent aphasia and focal left frontal operculo-insular-striatal damage, we demonstrated increased right parietal and temporal grey matter volume and perfusion, suggesting a liberation of contralateral posterior cortical function (Seeley *et al.*, 2008b). Like patients with frontotemporal dementia, children with autism, who feature social-emotional and anatomical deficits akin to bvFTD (Di Martino *et al.*, 2009a), may show superior posterior cortical functions manifesting as extraordinary artistic, arithmetic or mnemonic talent (Hou *et al.*, 2000; Treffert, 2009). In the present study, bvFTD showed increased left parietal DMN connectivity that correlated with reduced Salience Network connectivity in right frontoinsular, striatal and cingulate regions.

Intriguingly, a recent study demonstrated divergent frontotemporal dementia versus Alzheimer's disease connectivity results using graph theoretical analysis of resting-state EEG data (de Haan *et al.*, 2009). These authors showed that whereas Alzheimer's disease deviated from an optimal 'small-world' network structure toward a more random configuration, frontotemporal dementia showed an opposite trend toward a (perhaps excessively) ordered structure, especially within the posterior alpha rhythm. Although EEG lacks sufficient spatial resolution to interrogate specific anatomical networks, especially those (like the Salience Network) composed of subcortical and deep cortical structures, the more orderly posterior cortical covariance structure in frontotemporal dementia may represent an electrophysiological counterpart, at higher temporal resolution, to our ICN fMRI findings.

Relationship between ICN changes and disease severity

To assess whether ICN mapping might hold promise as a disease-monitoring biomarker, we sought correlations between regional ICN strength and bvFTD clinical severity. The results provided a striking network dissociation. Whereas worsening Salience Network right frontoinsula connectivity predicted greater disease severity, so too did increases in bilateral angular gyrus (ANG) connectivity within the DMN. These findings emphasize the centrality of right frontoinsula in anchoring the Salience Network (Seeley *et al.*, 2007b; Sridharan *et al.*, 2008) and in giving rise, when injured, to bvFTD functional deficits. The right

frontoinsula features the peak brain-wide concentration of von Economo neurons, large bipolar Layer V projection neurons shown to undergo early, selective degeneration in bvFTD but not in Alzheimer's disease (Seeley *et al.*, 2006, 2007a). Consistent with the present ICN findings, we recently found that selective von Economo neuron loss in the right (but not left) frontoinsula correlated with bvFTD clinical severity measured with the CDR-SB (Kim *et al.*, unpublished results). Sensitive, subject-level tracking of disease stage represents a major potential advantage of ICN fMRI over structural imaging, which may lag too far behind dynamic clinical and biological changes to prove useful for drug development.

ICN mapping as a diagnostic biomarker for neurodegenerative disease

We combined Salience Network and DMN connectivity scores to classify our three groups with 92% accuracy and separate bvFTD and Alzheimer's disease with 100% accuracy based on clinical diagnosis. This approach requires replication in an independent clinical dataset and validation in pathologically verified clinical samples. Available supportive biological data, however, strongly supported clinical diagnoses used to group patients in this study. Because other frontotemporal dementia syndromes, such as semantic dementia, progressive non-fluent aphasia and corticobasal syndrome also cause atrophy within specific ICNs (Seeley *et al.*, 2009), the present results warrant future direct ICN investigations of these disorders.

Reliable discrimination of frontotemporal dementia syndromes from Alzheimer's disease will become critical as disease modifying treatments emerge. Some patients present with prominent behavioural but also memory and spatial impairments, leading clinicians to waver diagnostically between bvFTD and Alzheimer's disease. Previous attempts to separate these disorders with imaging have yielded mixed results, and to our knowledge no previous method has provided 100% separation. Recently, a complex grey matter spatial pattern analysis achieved 100% separation of Alzheimer's disease or frontotemporal dementia from controls, but accuracy fell to 84% when applied to frontotemporal dementia versus Alzheimer's disease (Davatzikos *et al.*, 2008). Machine learning algorithms performed on single photon emission computed tomography images provided 88% accuracy for frontotemporal dementia versus Alzheimer's disease (Horn *et al.*, 2009). In the largest study to include a pathological gold standard, Foster *et al.* (2007) used PET with fluorodeoxyglucose (FDG-PET) to achieve 90% diagnostic accuracy for frontotemporal dementia versus Alzheimer's disease. In the present study, patients with typical bvFTD and Alzheimer's disease were classified with 100% accuracy, and four diagnostically controversial PIB-positive patients not used to train the algorithm were classified as Alzheimer's disease by our approach.

ICN fMRI biomarkers could provide several important advantages over existing functional-metabolic (FDG-PET) and molecular (PIB-PET) imaging methods. Though both PET techniques show promise for separating frontotemporal dementia from Alzheimer's disease (Foster *et al.*, 2007; Rabinovici *et al.*,

2007a), they remain invasive and costly, available only at selected centres, and repeatable only after a prolonged interval due to radioactivity exposure concerns. Furthermore, PET may lack the spatial resolution to detect focal limbic, subcortical or brainstem dysfunction and PIB-PET has failed to track clinical severity in patients with Alzheimer's disease (Scheinin *et al.*, 2009). In contrast, ICN fMRI provides a simple, non-invasive, inexpensive technique that adds less than 10 min to a standard clinical MRI scan routinely obtained to rule out non-degenerative structural disease. Furthermore, ICN fMRI provides an immediately repeatable and treatment-responsive (James *et al.*, 2009) method which, as shown in this study, proves sensitive to disease severity and may help discriminate between bvFTD and Alzheimer's disease. Finally, the task-free nature of ICN fMRI mitigates concerns relevant to implementing scanner-based fMRI tasks in patients with poor working memory, apathy or behavioural imperistence. No doubt owing to these issues, only one small task-based fMRI study of bvFTD has been published to date (Rombouts *et al.*, 2003). As ICN biomarker development moves forward, further information will be needed regarding how pharmacological conditions (scan-associated sedation or ongoing treatments) impact ICN strength.

Limitations and future directions

This study's major limitations relate to sample size, scanner variability and the lack of a large independent dataset to test our exploratory diagnostic classification algorithm. Twelve subjects per group, though sufficient to detect hypothesized group differences, proved too few to explore correlations between ICN strength and specific behavioural or neuropsychological variables of interest; we hope to pursue these goals in future studies. We accounted for scanner variability by matching groups for scan site and by including scan site as a confounding covariate in all analyses, following previous approaches (Kim *et al.*, 2009). Greatest caution should be applied to our diagnostic algorithm, which was initially trained and tested on the same subject pool, making it unlikely to perform as well on an independent clinical sample. Although the accurate classification of four diagnostically challenging independent 'test' patients is encouraging, future larger studies are needed to delineate the most discriminating and generalizable indices of ICN function and to confirm that ICNs prove reliable within subjects, as suggested by several recent studies (Fox *et al.*, 2007; Cohen *et al.*, 2008; Meindl *et al.*, 2009; Shehzad *et al.*, 2009). Increasingly advanced data-driven methods may help speed researchers towards these goals.

Acknowledgements

The authors thank Richard C. Crawford, Katherine Prater, Victor Laluz, Christopher Ching and Rudolph Walter for technical assistance with data collection and storage, William J. Jagust for PIB-PET imaging, and A.D. (Bud) Craig for discussion. Finally, we thank our patients and their families for their generous contributions to neurodegeneration research.

Funding

National Institute of Aging (NIA grant number K08 AG027086 to W.W.S., P01 AG19724 and P50 AG1657303-75271 to B.L.M., R01-AG027859 to William J. Jagust, and K23-AG031861 to G.D.R.); the National Institute of Neurological Disorders and Stroke (NINDS grant number K23NS048302 to M.D.G.); Alzheimer's Association (grant number NIRG-07-59422 to G.D.R.); and the Larry L. Hillblom Foundation (grant number 2005/2T to W.W.S.).

Supplementary material

Supplementary material is available at *Brain* online.

References

- Aizenstein HJ, Nebes RD, Saxton JA, Price JC, Mathis CA, Tsopelas ND, et al. Frequent amyloid deposition without significant cognitive impairment among the elderly. *Arch Neurol* 2008; 65: 1509–17.
- Beckmann CF, Smith SM. Probabilistic independent component analysis for functional magnetic resonance imaging. *Med Imaging IEEE Trans* 2004; 23: 137–52.
- Beckmann CF, DeLuca M, Devlin JT, Smith SM. Investigations into resting-state connectivity using independent component analysis. *Philos Trans R Soc Lond B Biol Sci* 2005; 360: 1001–13.
- Belgrave M. The effect of expressive and instrumental touch on the behavior states of older adults with late-stage dementia of the Alzheimer's type and on music therapist's perceived rapport. *J Music Ther* 2009; 46: 132–46.
- Benoit M, Dygai I, Migneco O, Robert PH, Bertogliati C, Darcourt J, et al. Behavioral and psychological symptoms in Alzheimer's disease. *Dement Geriatr Cogn Disord* 1999; 10: 511–7.
- Boccardi M, Sabatoli F, Laakso MP, Testa C, Rossi R, Beltramello A, et al. Frontotemporal dementia as a neural system disease. *Neurobiol Aging* 2005; 26: 37–44.
- Brambati SM, Renda NC, Rankin KP, Rosen HJ, Seeley WW, Ashburner J, et al. A tensor based morphometry study of longitudinal gray matter contraction in FTD. *Neuroimage* 2007; 35: 998–1003.
- Broe M, Hodges JR, Schofield E, Shepherd CE, Kril JJ, Halliday GM. Staging disease severity in pathologically confirmed cases of frontotemporal dementia. *Neurology* 2003; 60: 1005–11.
- Brun A, Liu X, Erikson C. Synapse loss and gliosis in the molecular layer of the cerebral cortex in Alzheimer's disease and in frontal lobe degeneration. *Neurodegeneration* 1995; 4: 171–7.
- Buckner RL, Snyder AZ, Shannon BJ, LaRossa G, Sachs R, Fotenos AF, et al. Molecular, structural, and functional characterization of Alzheimer's disease: evidence for a relationship between default activity, amyloid, and memory. *J Neurosci* 2005; 25: 7709–17.
- Casanova R, Srikanth R, Baer A, Laurienti PJ, Burdette JH, Hayasaka S, et al. Biological parametric mapping: a statistical toolbox for multimodality brain image analysis. *Neuroimage* 2007; 34: 137–43.
- Cavanna AE, Trimble MR. The precuneus: a review of its functional anatomy and behavioural correlates. *Brain* 2006; 129: 564–83.
- Cohen AL, Fair DA, Dosenbach NUF, Miezin FM, Dierker D, Van Essen DC, et al. Defining functional areas in individual human brains using resting functional connectivity MRI. *Neuroimage* 2008; 41: 45–57.
- Cole LJ, Farrell MJ, Duff EP, Barber JB, Egan GF, Gibson SJ. Pain sensitivity and fMRI pain-related brain activity in Alzheimer's disease. *Brain* 2006; 129: 2957–65.
- Craig AD. Emotional moments across time: a possible neural basis for time perception in the anterior insula. *Philos Trans R Soc Lond B Biol Sci* 2009a; 364: 1933–42.
- Craig AD. How do you feel—now? The anterior insula and human awareness. *Nat Rev Neurosci* 2009b; 10: 59–70.
- Damasio AR. Feelings of emotion and the self. *Ann NY Acad Sci* 2003; 1001: 253–61.
- Damoiseaux JS, Rombouts SARB, Barkhof F, Scheltens P, Stam CJ, Smith SM, et al. Consistent resting-state networks across healthy subjects. *Proc Natl Acad Sci USA* 2006; 103: 13848–53.
- Davatzikos C, Resnick SM, Wu X, Pampi P, Clark CM. Individual patient diagnosis of AD and FTD via high-dimensional pattern classification of MRI. *NeuroImage* 2008; 41: 1220–7.
- de Haan W, Pijnenburg Y, Strijers R, van der Made Y, van der Flier W, Scheltens P, et al. Functional neural network analysis in frontotemporal dementia and Alzheimer's disease using EEG and graph theory. *BMC Neuroscience* 2009; 10: 101.
- Di Martino A, Ross K, Uddin LQ, Sklar AB, Castellanos FX, Milham MP. Functional brain correlates of social and nonsocial processes in autism spectrum disorders: an activation likelihood estimation meta-analysis. *Biol Psychiatry* 2009a; 65: 63–74.
- Di Martino A, Shehzad Z, Kelly C, Roy AK, Gee DG, Uddin LQ, et al. Relationship between cingulo-insular functional connectivity and autistic traits in neurotypical adults. *Am J Psychiatry* 2009b; 166: 891–9.
- Eslinger PJ, Dennis K, Moore P, Antani S, Hauck R, Grossman M. Metacognitive deficits in frontotemporal dementia. *J Neurol Neurosurg Psychiatry* 2005; 76: 1630–5.
- Filippini N, MacIntosh BJ, Hough MG, Goodwin GM, Frisoni GB, Smith SM, et al. Distinct patterns of brain activity in young carriers of the APOE-epsilon4 allele. *Proc Natl Acad Sci USA* 2009; 106: 7209–14.
- Fleisher AS, Sherzai A, Taylor C, Langbaum JBS, Chen K, Buxton RB. Resting-state BOLD networks versus task-associated functional MRI for distinguishing Alzheimer's disease risk groups. *NeuroImage* 2009; 47: 1678–90.
- Foster NL, Heidebrink JL, Clark CM, Jagust WJ, Arnold SE, Barbas NR, et al. FDG-PET improves accuracy in distinguishing frontotemporal dementia and Alzheimer's disease. *Brain* 2007; 130: 2616–35.
- Fox MD, Snyder AZ, Vincent JL, Corbetta M, Van Essen DC, Raichle ME. The human brain is intrinsically organized into dynamic, anticorrelated functional networks. *Proc Natl Acad Sci USA* 2005; 102: 9673–8.
- Fox MD, Raichle ME. Spontaneous fluctuations in brain activity observed with functional magnetic resonance imaging. *Nat Rev Neurosci* 2007; 8: 700–11.
- Fox MD, Snyder AZ, Vincent JL, Raichle ME. Intrinsic fluctuations within cortical systems account for intertrial variability in human behavior. *Neuron* 2007; 56: 171–84.
- Fransson P. Spontaneous low-frequency BOLD signal fluctuations: an fMRI investigation of the resting-state default mode of brain function hypothesis. *Hum Brain Mapp* 2005; 26: 15–29.
- Good CD, Johnsrude IS, Ashburner J, Henson RN, Friston KJ, Frackowiak RS. A voxel-based morphometric study of ageing in 465 normal adult human brains. *Neuroimage* 2001; 14(1 Pt 1): 21–36.
- Greicius MD, Krasnow B, Reiss AL, Menon V. Functional connectivity in the resting brain: a network analysis of the default mode hypothesis. *Proc Natl Acad Sci USA* 2003; 100: 253–8.
- Greicius MD, Menon V. Default-mode activity during a passive sensory task: uncoupled from deactivation but impacting activation. *J Cogn Neurosci* 2004; 16: 1484–92.
- Greicius MD, Srivastava G, Reiss AL, Menon V. Default-mode network activity distinguishes Alzheimer's disease from healthy aging: evidence from functional MRI. *Proc Natl Acad Sci USA* 2004; 101: 4637–42.
- Grinberg LT, Rub U, Ferretti RE, Nitri R, Farfel JM, Polichio L, et al. The dorsal raphe nucleus shows phospho-tau neurofibrillary changes before the transentorhinal region in Alzheimer's disease. A precocious onset? *Neuropathol Appl Neurobiol* 2009; 35: 406–16.

- Habas C, Kamdar N, Nguyen D, Prater K, Beckmann CF, Menon V, et al. Distinct cerebellar contributions to intrinsic connectivity networks. *J Neurosci* 2009; 29: 8586–94.
- Hampson M, Driesen NR, Skudlarski P, Gore JC, Constable RT. Brain Connectivity Related to Working Memory Performance. *J Neurosci* 2006; 26: 13338–43.
- He Y, Wang L, Zang Y, Tian L, Zhang X, Li K, et al. Regional coherence changes in the early stages of Alzheimer's disease: a combined structural and resting-state functional MRI study. *Neuroimage* 2007; 35: 488–500.
- Heimer L, Van Hoesen GW. The limbic lobe and its output channels: implications for emotional functions and adaptive behavior. *Neurosci Biobehav Rev* 2006; 30: 126–47.
- Helmich RC, Derix LC, Bakker M, Scheeringa R, Bloem BR, Toni I. Spatial Remapping of Cortico-striatal Connectivity in Parkinson's Disease. *Cereb Cortex* 2009. Advance Access published on August 29, 2009, doi:10.1093/cercor/bhp178.
- Hodges JR, Davies RR, Xuereb JH, Casey B, Broe M, Bak TH, et al. Clinicopathological correlates in frontotemporal dementia. *Ann Neurol* 2004; 56: 399–406.
- Horn J-F, Habert M-O, Kas A, Malek Z, Maksud P, Lacomblez L, et al. Differential automatic diagnosis between Alzheimer's disease and frontotemporal dementia based on perfusion SPECT images. *Artificial Int Med* 2009; 47: 147–58.
- Hou C, Miller BL, Cummings J, Goldberg M, Mychack P, Bottino V, et al. Autistic savants. [correction of artistic]. *Neuropsychiatry Neuropsychol Behav Neurol* 2000; 13: 29–38.
- James A, Lu Z-L, VanMeter J, Sathian K, Sathian M, Hu X, et al. Changes in resting state effective connectivity in the motor network following rehabilitation of upper extremity poststroke paresis. *Topics Stroke Rehab* 2009; 16: 270–81.
- Kim DH, Adalsteinsson E, Glover GH, Spielman S. SVD regularization algorithm for improved high-order shimming. Denver. 2000; p. 1685.
- Kim DI, Mathalon DH, Ford JM, Mannell M, Turner JA, Brown GG, et al. Auditory oddball deficits in Schizophrenia: an independent component analysis of the fMRI multisite function BIRN study. *Schizophr Bull* 2009; 35: 67–81.
- Kiviniemi VJ, Haanpaa H, Kantola J-H, Jauhiainen J, Vainionpaa V, Alahuhta S, et al. Midazolam sedation increases fluctuation and synchrony of the resting brain BOLD signal. *Magn Reson Imaging* 2005; 23: 531–7.
- Lough S, Kipps CM, Treise C, Watson P, Blair JR, Hodges JR. Social reasoning, emotion and empathy in frontotemporal dementia. *Neuropsychologia* 2006; 44: 950–8.
- Matsuda H, Kanetaka H, Ohnishi T, Asada T, Imabayashi E, Nakano S, et al. Brain SPET abnormalities in Alzheimer's disease before and after atrophy correction. *Eur J Nuclear Med Mol Imaging* 2002; 29: 1502–5.
- McKhann G, Drachman D, Folstein M, Katzman R, Price D, Stadlan EM. Clinical diagnosis of Alzheimer's disease: report of the NINCDS-ADRDA Work Group under the auspices of Department of Health and Human Services Task Force on Alzheimer's Disease. *Neurology* 1984; 34: 939–44.
- Mega MS, Cummings JL, Fiorello T, Gornbein J. The spectrum of behavioral changes in Alzheimer's disease. *Neurology* 1996; 46: 130–5.
- Meindl T, Teipel S, Elmouden R, Mueller S, Koch W, Dietrich O, et al. Test-retest reproducibility of the default-mode network in healthy individuals. *Hum Brain Mapp* 2009; 31: 237–46.
- Mendez MF, Cherrier M, Perryman KM, Pachana N, Miller BL, Cummings JL. Frontotemporal dementia versus Alzheimer's disease: differential cognitive features. *Neurology* 1996; 47: 1189–94.
- Mendez MF, Shapira JS. Altered emotional morality in frontotemporal dementia. *Cogn Neuropsychiatry* 2009; 14: 165–79.
- Mesulam MM, Mufson EJ. Insula of the old world monkey. III: efferent cortical output and comments on function. *J Comp Neurol* 1982; 212: 38–52.
- Mesulam MM. From sensation to cognition. *Brain* 1998; 121(Pt 6): 1013–52.
- Meyer-Lindenberg A, Mervis CB, Faith Berman K. Neural mechanisms in Williams syndrome: a unique window to genetic influences on cognition and behaviour. *Nat Rev Neurosci* 2006; 7: 380–93.
- Miller BL, Ponton M, Benson DF, Cummings JL, Mena I. Enhanced artistic creativity with temporal lobe degeneration. *Lancet* 1996; 348: 1744–5.
- Miller BL, Cummings J, Mishkin F, Boone K, Prince F, Ponton M, et al. Emergence of artistic talent in frontotemporal dementia. *Neurology* 1998; 51: 978–82.
- Miller BL, Boone K, Cummings JL, Read SL, Mishkin F. Functional correlates of musical and visual ability in frontotemporal dementia. *Br J Psychiatry* 2000; 176: 458–63.
- Mohammadi B, Kollewe K, Samii A, Krampfl K, Dengler R, Münte TF. Changes of resting state brain networks in amyotrophic lateral sclerosis. *Exp Neurol* 2009; 217: 147–53.
- Neary D, Snowden JS, Gustafson L, Passant U, Stuss D, Black S, et al. Frontotemporal lobar degeneration: a consensus on clinical diagnostic criteria. *Neurology* 1998; 51: 1546–54.
- Ongur D, Price JL. The organization of networks within the orbital and medial prefrontal cortex of rats, monkeys and humans. *Cereb Cortex* 2000; 10: 206–19.
- Poline JB, Worsley KJ, Evans AC, Friston KJ. Combining spatial extent and peak intensity to test for activations in functional imaging. *Neuroimage* 1997; 5: 83–96.
- Rabinovici GD, Furst AJ, O'Neil JP, Racine CA, Mormino EC, Baker SL, et al. 11C-PIB PET imaging in Alzheimer disease and frontotemporal lobar degeneration. *Neurology* 2007a; 68: 1205–12.
- Rabinovici GD, Seeley WW, Kim EJ, Gorno-Tempini ML, Rascovsky K, Pagliaro TA, et al. Distinct MRI atrophy patterns in autopsy-proven Alzheimer's disease and frontotemporal lobar degeneration. *Am J Alzheimers Dis Other Dement* 2007b; 22: 474–88.
- Raichle M, MacLeod A, Snyder A, Powers W, Gusnard D, Shulman G. Inaugural Article: a default mode of brain function. *Proc Natl Acad Sci USA* 2001; 98: 676.
- Rankin KP, Kramer JH, Miller BL. Patterns of cognitive and emotional empathy in frontotemporal lobar degeneration. *Cogn Behav Neurol* 2005; 18: 28–36.
- Rankin KP, Gorno-Tempini ML, Allison SC, Stanley CM, Glenn S, Weiner MW, et al. Structural anatomy of empathy in neurodegenerative disease. *Brain* 2006; 129: 2945–56.
- Ratnavalli E, Brayne C, Dawson K, Hodges JR. The prevalence of frontotemporal dementia. *Neurology* 2002; 58: 1615–21.
- Rohrer JD, Warren JD, Omar R, Mead S, Beck J, Revesz T, et al. Parietal lobe deficits in frontotemporal lobar degeneration caused by a mutation in the progranulin gene. *Arch Neurol* 2008; 65: 506–13.
- Rombouts SA, van Swieten JC, Pijnenburg YA, Goekoop R, Barkhof F, Scheltens P. Loss of frontal fMRI activation in early frontotemporal dementia compared to early AD. *Neurology* 2003; 60: 1904–8.
- Rombouts SARB, Barkhof F, Goekoop R, Stam CJ, Scheltens P. Altered resting state networks in mild cognitive impairment and mild Alzheimer's disease: an fMRI study. *Human Brain Mapp* 2005; 26: 231–9.
- Rosen HJ, Gorno-Tempini ML, Goldman WP, Perry RJ, Schuff N, Weiner M, et al. Patterns of brain atrophy in frontotemporal dementia and semantic dementia. *Neurology* 2002; 58: 198–208.
- Rosen HJMD, Narvaez JMBS, Hallam BP, Kramer JHP, Wyss-Coray CRN, Gearhart RMSNCS, et al. Neuropsychological and functional measures of severity in Alzheimer disease, frontotemporal dementia, and semantic dementia. *Alzheimer Dis Assoc Disord* 2004; 18: 202–7.
- Rub U, Del Tredici K, Schultz C, Thal DR, Braak E, Braak H. The evolution of Alzheimer's disease-related cytoskeletal pathology in the human raphe nuclei. *Neuropathol Appl Neurobiol* 2000; 26: 553–67.
- Salvador R, Suckling J, Coleman MR, Pickard JD, Menon D, Bullmore E. Neurophysiological architecture of functional magnetic resonance images of human brain. *Cereb Cortex* 2005; 15: 1332–42.

- Sampathu DM, Neumann M, Kwong LK, Chou TT, Micsenyi M, Truax A, et al. Pathological heterogeneity of frontotemporal lobar degeneration with ubiquitin-positive inclusions delineated by ubiquitin immunohistochemistry and novel monoclonal antibodies. *Am J Pathol* 2006; 169: 1343–52.
- Saper CB. The central autonomic nervous system: conscious visceral perception and autonomic pattern generation. *Annu Rev Neurosci* 2002; 25: 418–69.
- Scheinin NM, Aalto S, Koikkalainen J, Lotjonen J, Karrasch M, Kempainen N, et al. Follow-up of [¹¹C]PIB uptake and brain volume in patients with Alzheimer disease and controls. *Neurology* 2009; 73: 1186–92.
- Schroeter ML, Raczka K, Neumann J, von Cramon DY. Neural networks in frontotemporal dementia - a meta-analysis. *Neurobiol Aging* 2008; 29: 418–26.
- Seeley WW, Carlin DA, Allman JM, Macedo MN, Bush C, Miller BL, et al. Early frontotemporal dementia targets neurons unique to apes and humans. *Ann Neurol* 2006; 60: 660–7.
- Seeley WW, Allman JM, Carlin DA, Crawford RK, Macedo MN, Greicius MD, et al. Divergent social functioning in behavioral variant frontotemporal dementia and Alzheimer disease: reciprocal networks and neuronal evolution. *Alzheimer Dis Assoc Disord* 2007a; 21: S50–7.
- Seeley WW, Menon V, Schatzberg AF, Keller J, Glover GH, Kenna H, et al. Dissociable intrinsic connectivity networks for salience processing and executive control. *J Neurosci* 2007b; 27: 2349–56.
- Seeley WW. Selective functional, regional, and neuronal vulnerability in frontotemporal dementia. *Curr Opin Neurol* 2008; 21: 701–7.
- Seeley WW, Crawford R, Rascofsky K, Kramer JH, Weiner M, Miller BL, et al. Frontal paralimbic network atrophy in very mild behavioral variant frontotemporal dementia. *Arch Neurol* 2008a; 65: 249–55.
- Seeley WW, Matthews BR, Crawford RK, Gorno-Tempini ML, Foti D, Mackenzie IR, et al. Unravelling Bolero: progressive aphasia, transmodal creativity and the right posterior neocortex. *Brain* 2008b; 131(Pt 1): 39–49.
- Seeley WW, Crawford RK, Zhou J, Miller BL, Greicius MD. Neurodegenerative diseases target large-scale human brain networks. *Neuron* 2009; 62: 42–52.
- Senjem ML, Gunter JL, Shiung MM, Petersen RC, Jack CR Jr. Comparison of different methodological implementations of voxel-based morphometry in neurodegenerative disease. *Neuroimage* 2005; 26: 600–8.
- Shehzad Z, Kelly AM, Reiss PT, Gee DG, Gotimer K, Uddin LQ, et al. The resting brain: unconstrained yet reliable. *Cereb Cortex* 2009; 19: 2209–29.
- Sorg C, Riedel V, Muhlau M, Calhoun VD, Eichele T, Laer L, et al. Selective changes of resting-state networks in individuals at risk for Alzheimer's disease. *Proc Natl Acad Sci USA* 2007; 104: 18760–5.
- Sridharan D, Levitin DJ, Menon V. A critical role for the right fronto-insular cortex in switching between central-executive and default-mode networks. *Proc Natl Acad Sci USA* 2008; 105: 12569–74.
- Sturm VE, Rosen HJ, Allison S, Miller BL, Levenson RW. Self-conscious emotion deficits in frontotemporal lobar degeneration. *Brain* 2006; 129(Pt 9): 2508–16.
- Sturm VE, Ascher EA, Miller BL, Levenson RW. Diminished self-conscious emotional responding in frontotemporal lobar degeneration patients. *Emotion* 2008; 8: 861–9.
- Supekar K, Menon V, Rubin D, Musen M, Greicius MD. Network analysis of intrinsic functional brain connectivity in Alzheimer's disease. *PLoS Comput Biol* 2008; 4: e1000100.
- Sutton BP, Goh J, Hebrank A, Welsh RC, Chee MWL, Park DC. Investigation and validation of intersite fMRI studies using the same imaging hardware. *J MRI* 2008; 28: 21–8.
- Taylor KS, Seminowicz DA, Davis KD. Two systems of resting state connectivity between the insula and cingulate cortex. *Hum Brain Mapp* 2009; 30: 2731–45.
- Treffert DA. The savant syndrome: an extraordinary condition. A synopsis: past, present, future. *Philos Trans R Soc B Biol Sci* 2009; 364: 1351–7.
- Tzourio-Mazoyer N, Landeau B, Papathanassiou D, Crivello F, Etard O, Delcroix N, et al. Automated anatomical labeling of activations in SPM using a macroscopic anatomical parcellation of the MNI MRI single-subject brain. *NeuroImage* 2002; 15: 273–89.
- Vincent JL, Patel GH, Fox MD, Snyder AZ, Baker JT, Van Essen DC, et al. Intrinsic functional architecture in the anaesthetized monkey brain. *Nature* 2007; 447: 83–6.
- Wu T, Wang L, Chen Y, Zhao C, Li K, Chan P. Changes of functional connectivity of the motor network in the resting state in Parkinson's disease. *Neurosci Lett* 2009; 460: 6–10.
- Zysset S, Huber O, Ferstl E, von Cramon DY. The anterior frontomedian cortex and evaluative judgment: an fMRI study. *Neuroimage* 2002; 15: 983–91.